

Airborne laser fluorosensing of maritime parameters: application of geostatistics

W. Milchers, S. Patsayeva⁺, R. Reuter and R. Willkomm

Carl von Ossietzky Universität Oldenburg, FB Physik, D-26111 Oldenburg, Germany
email: (r.reuter, willkomm)@las.physik.uni-oldenburg.de

⁺ Moscow State University, Physics Department, Moscow, 119899 Russia
email: svetlana@lidar.phys.msu.su

ABSTRACT

By the end of 1993 the Federal Ministries of Transport and Defence put a second generation maritime surveillance system into service for long-term operation in the North Sea and the Baltic Sea. The system consists of a DO 228-212 aircraft and of a side-looking airborne radar, a microwave radiometer, a UV/IR line scanner, and a laser fluorosensor.

The main purpose of the laser fluorosensor is the detection classification and volume estimation of oil spills on the sea surface. In addition, gelbstoff and phytoplankton pigments can be investigated while the aircraft is performing long-range surveillance flights. These maritime data are analysed by geostatistical algorithms, which exploit the spatial correlation of the data to estimate the 2-dimensional distribution of the examined property. As an additional information about the reliability of the results, the prediction variance is accessible. In this way, a detailed illustration of maritime conditions in coastal waters can be achieved. In this article, we discuss problems that arise if the condition of statistical uniformity is not met by the data. A possible way to handle these data is demonstrated on a data set measured in the North Sea.

1. INTRODUCTION

In 1993 a Dornier DO 282-212 aircraft was procured for maritime surveillance by the Federal Ministry of Transport and by the Federal Coastal States of Bremen, Hamburg, Lower Saxony and Sleswig-Holstein.¹ Operated by the Naval Air Wing 3 in Nordholz, this aircraft is equipped with side-looking airborne radar (SLAR) for detecting oil slicks over large distances, a UV/IR scanner, and a microwave radiometer for mapping the sea surface in the nadir range, and a scanning laser fluorosensor.²

In addition to oil spill parameters like film thickness estimation and oil type classification,³ the laser fluorosensor signals contain information about some ecologically relevant properties such as seawater attenuation coefficients, and concentrations of phytoplankton and gelbstoff (i.e. dissolved organic matter),

as reviewed by Measures.⁴ These parameters are useful to describe the ecological state of coastal waters like e.g. the North Sea.⁵

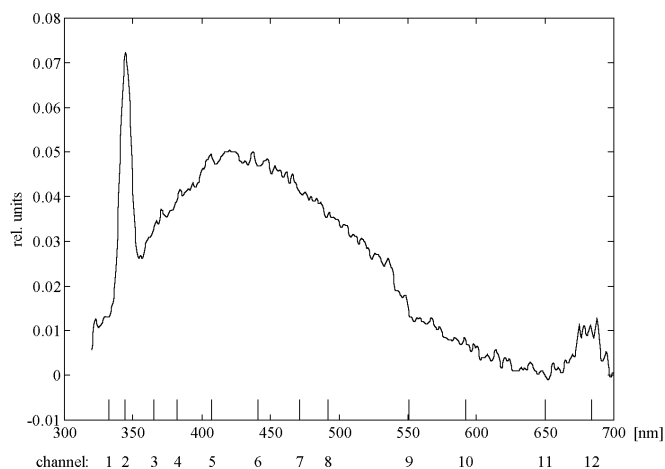


Fig. 1: Typical fluorescence emission spectrum of seawater, measured with a laboratory spectrofluorometer at 308 nm excitation wavelength. LFS detection channels² are indicated. The peak at 344 nm is water Raman scattering. The bands with maxima at 420 and 680 nm are due to gelbstoff and phytoplankton chlorophyll fluorescence.

With airborne laser fluorosensors, data are measured along the flight track of the aircraft. An estimate of the distribution of the measured properties in a larger area necessitates an interpolation between and extrapolation outside the flight tracks. This can be achieved with geostatistical tools,^{6,7} a set of statistical algorithms for the analysis and gridding of scattered spatial data. In this paper, we report on the calculation of two-dimensional maps of hydrographic parameters, based on the geostatistical interpolation of airborne LFS data. The performance of geostatistics is optimal if data are multivariate normal distributed, at least statistical uniformity has to be assumed. If this requirement is not met by the data, one can apply the so-called indicator kriging that is reported to be stable against deviations from this assumption.⁸ Another approach is the trans-

formation to normality prior to the geostatistical computations, which we have tested on airborne fluorescence data.

2. REGIONALISED VARIABLES

In this section we will briefly present the basic concepts of geostatistics. A complete description can be found in Journé and Huijbregts.⁶ The theory of geostatistics was founded in France by G. Matheron based on ideas of D. Krige. The first purpose of these techniques was in the mining industry, to estimate ore concentrations. During the eighties many more fields of application were found, for example in hydrology, in environmetrics and in remote sensing.

The background of geostatistics is the concept of regionalised variables. Each data point $z(x_i)$ is viewed as a realisation of a probability process,

$$Z(x_i) = m(x_i) + V(x_i), i = 1..n,$$

divided into a slowly varying mean value $m(x)$ and an error process $V(x_i)$ that represents the local deviations from the mean. The mean

$$m(x_i) = E[Z(x_i)] = \sum_{k=1}^p \beta_k f_k(x_i)$$

can be expressed as a linear combination of p basis functions $f_j(x_i)$, e.g. polynoms, and the covariance

$C(x_i, x_j)$ or the semivariogram $\gamma(x_i, x_j)$:

$$C(x_i, x_j) = E[V(x_i) \cdot V(x_j)]$$

$$\gamma(x_i, x_j) = \frac{1}{2} E[(V(x_i) - V(x_j))^2]$$

The semivariogram characterises the spatial correlation between adjacent measurements. In general a variogram or covariance model is fitted to the data, for example a Gaussian model:

$$\gamma(h) = \theta_0 + \theta_1 \cdot \exp\left(-\frac{h^2}{\theta_2}\right),$$

where h is the distance between measurements. We have mainly used Restricted-Maximum-Likelihood (RML) estimators⁹ to fit the variogram parameters $\theta_1 \dots \theta_3$. With the assumption of spatial homogeneity this information can be exploited for the estimation of values of the measured property at locations where data are not available. This is done in an optimal way with kriging. The kriging estimator $\hat{Z}(x)$ is the best linear unbiased estimator (BLUE)⁹ in cases where the semivariogram is known. The estimate $\hat{z}(x_k)$ is a weighted average of the whole data set or of a subset in the neighbourhood of x_k :

$$\hat{z}(x_k) = \sum_{i=1}^n \omega_i z(x_i) = \boldsymbol{\omega}^T \mathbf{z}$$

The unknown weights $\boldsymbol{\omega}$ are calculated with the kriging equation system:

$$\begin{pmatrix} \mathbf{C} & \mathbf{B} \\ \mathbf{B}^T & \mathbf{0} \end{pmatrix} \cdot \begin{pmatrix} \boldsymbol{\omega} \\ \boldsymbol{\lambda} \end{pmatrix} = \begin{pmatrix} \mathbf{c}_0 \\ \mathbf{b}_0^T \end{pmatrix},$$

\mathbf{C} : $n \times n$ matrix of the covariances between the data points,

\mathbf{c}_0 : $n \times 1$ vector of the covariances between the data points and the prediction location,

\mathbf{B} : $n \times p$ matrix which columns consist of the base functions evaluated at the location of the data points,

\mathbf{b}_0 : $1 \times p$ vector of the base functions evaluated at the prediction location x ,

$\boldsymbol{\lambda}$: $p \times 1$ vector of Lagrange multipliers.

The prediction variance is then:

$$\hat{\sigma}(x) = C(x, x) - \boldsymbol{\omega}^T \mathbf{c}_0 + \mathbf{b}_0 \boldsymbol{\lambda}.$$

Inaccuracies occur if the variance is a function of the position since there is no simple means to take into account information about local noise in the kriging estimator and in the estimation variance. Especially the predicted variance is strongly biased in these cases. A possible way to solve this problem can be a transformation to a multivariate normal distribution prior to the geostatistical computations. Then a spatial anisotropy of the variance disappears, and this can be considered as an optimal preparation of the data.

An algorithm to find a nearly optimal transformation rule was introduced by Box and Cox.¹⁰ The transformed data set is derived from the original one with the equation

$$y(x_i) = \begin{cases} \frac{z(x_i)^\rho - 1}{\rho} & \text{if } \rho \neq 0 \\ \log(z(x_i)) & \text{if } \rho = 0 \end{cases}, i = 1..n$$

where the parameter ρ has to be chosen in an optimal way. Box and Cox introduced the criteria

$$L(\rho) = -\frac{n}{2} \log(SS/n) + (\rho - 1) \sum_{i=1}^n \log(z_i)$$

$$SS = \mathbf{y}^T (\mathbf{I} - \mathbf{X}(\mathbf{X}^T \mathbf{X})^{-1} \mathbf{X}^T) \mathbf{y}$$

which have to be maximised. $L(\rho)$ is similar to the likelihood of a multivariate normal distribution without any non-zero cross-covariances.

An alternative approach is the transformation to an exact univariate normal distribution,⁸ but there are some advantages of the Box-Cox transformation:

- it can be expressed as a simple formula. This simplifies the inverse transformation of results which are outside the range of the transformed data values, although the transformation rule is not necessarily optimal in such cases.

- it allows an easier incorporation of a trend to the data. The transformed data can be processed with the geostatistical tools, later-on followed by an inverse transformation of the results to the original scale:

$$\hat{z}(x) = \begin{cases} (\rho \cdot \hat{y}(x) + 1)^{1/\rho} & \text{if } \rho \neq 0 \\ \exp(\hat{y}(x)) & \text{if } \rho = 0 \end{cases}$$

The re-transformed kriging estimator has to be interpreted as the median instead of the expectation value, because the probability distribution on the original scale is not necessarily symmetric.

To obtain information about the estimation uncertainty one can calculate the Q(0.16) and Q(0.84) quantiles with the kriging estimator and the standard prediction deviation:

$$Q(0.16)_z(x) = \begin{cases} (\rho \cdot (\hat{y}(x) - \hat{\sigma}_y(x)) + 1)^{1/\rho} & \text{if } \rho \neq 0 \\ \exp(\hat{y}(x) - \hat{\sigma}_y(x)) & \text{if } \rho = 0 \end{cases}$$

$$Q(0.84)_z(x) = \begin{cases} (\rho \cdot (\hat{y}(x) + \hat{\sigma}_y(x)) + 1)^{1/\rho} & \text{if } \rho \neq 0 \\ \exp(\hat{y}(x) + \hat{\sigma}_y(x)) & \text{if } \rho = 0 \end{cases}$$

A quantile Q(a) of a distribution is a value which exceeds a · 100% of all values. The difference between the quantiles given above can replace the standard deviation as a measure of uncertainty.

An important task of any geostatistical analysis is the model validation: results can be considered reliable only if *a priori* assumptions like the trend model and the semivariogram are adequate. An often used diagnostic tool is the cross validation. It consists of the estimation of data values from the rest of the data set. This allows to calculate the standard residuals:¹¹

$$s(x_i) = \frac{\hat{z}(x_i) - z(x_i)}{\hat{\sigma}(x_i)^{1/2}}$$

Theoretically, these residuals should have an expectation value of zero and a variance of one, and they should not depend on the position of the measurement. Further improvements of the diagnostic results can be obtained with the orthogonal residuals¹⁰ which are independent of each other. This has a positive influence on the performance of statistical tests.

3. THE DATA SET AND RESULTS

The typical emission spectrum of a North Sea water sample excited at 308 nm, the wavelength of the XeCl excimer laser, is illustrated in Fig. 1 together with the spectral positions of the 12 channel detector of the LFS. The peak of water Raman scattering is at 344 nm (channel 2). A broad fluorescence maximum caused by gelbstoff is at about 440 nm (channel 5) and chlorophyll fluorescence at 685 nm (channel 12). The first step of the data evaluation is the normalisation of these fluorescence signals to the water Raman scatter intensity. This corrects the fluorescence readings for variations of the penetration depth of laser light in different water types.¹²

As an example of a set of airborne fluorosensor measurements we present the results from a mission on Sept. 13th, 1995 in the German Bight. This region is characterised by high loads of suspended particles and

gelbstoff, typical for many other turbid coastal waters. The flight track and a plot of the water Raman normalised gelbstoff fluorescence is shown in Figs. 2 and 3. The main features are high concentrations and a high variability near the coast due to the freshwater input through rivers Elbe and Weser, and a more uniform distribution offshore. These rivers and the tidal flats of the Wadden Sea are the main source of gelbstoff in this region. As pointed out above, this heterogeneity of the variance reduces the applicability of geostatistics because it offends the assumption of a spatial independence of the semivariogram.

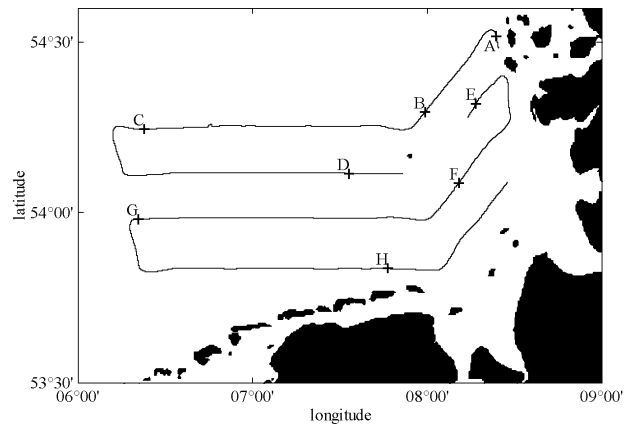


Fig. 2: Flight track of a survey in the German Bight, Sept 13th., 1995.

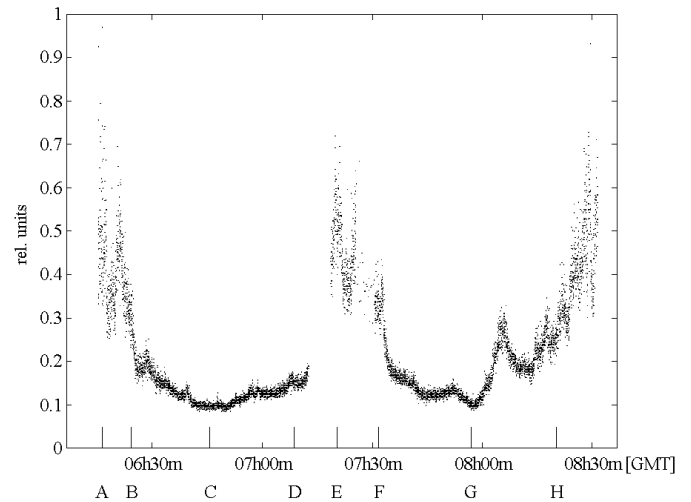


Fig. 3: Gelbstoff fluorescence normalised to water Raman scattering. Letters correspond to geographical positions given in Fig.1.

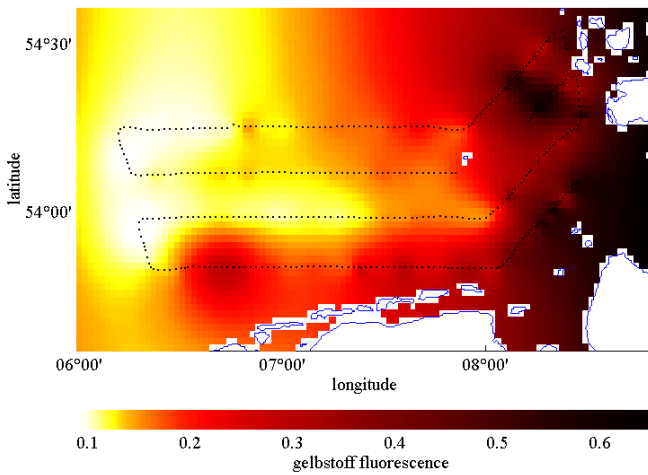


Fig. 4: Kriging predictor of the gelbstoff distribution in the German Bight. Excitation at 308 nm, emission at 440 nm. Survey on Sept 13th., 1995 (see Fig 2).

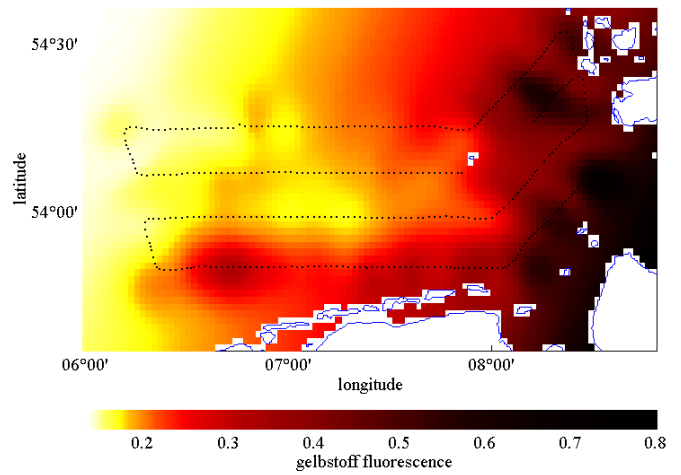


Fig. 7: Kriging predictor of the gelbstoff distribution derived with transformed data.

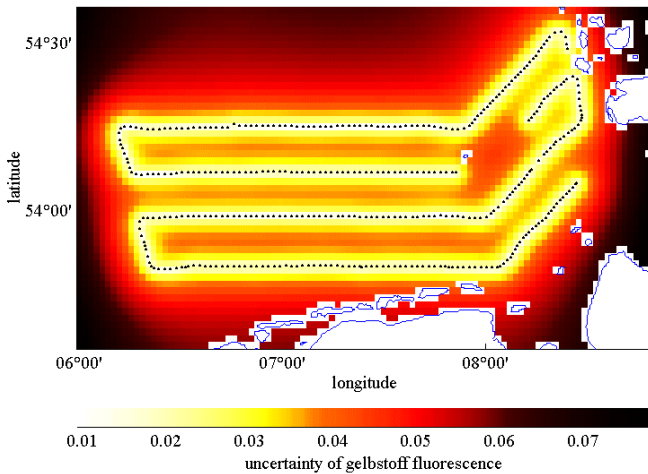


Fig. 5: Uncertainty of the distribution of gelbstoff fluorescence shown in Fig. 4.

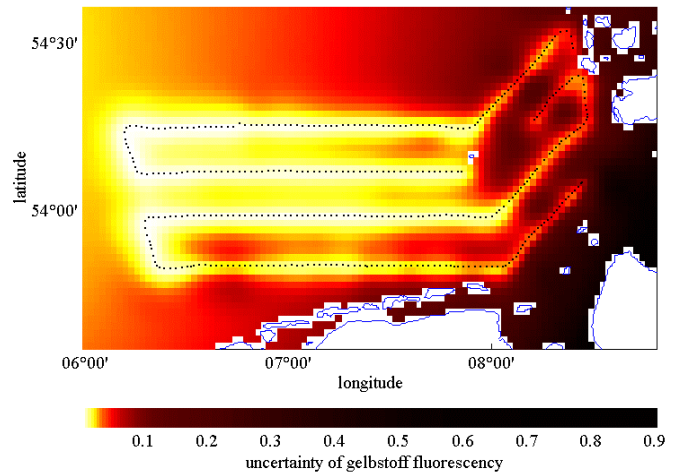


Fig. 8: Uncertainty of the distribution of gelbstoff fluorescence shown in Fig. 7.

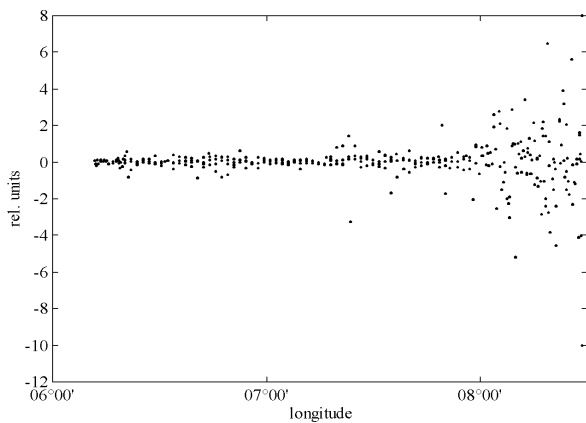


Fig. 6: Orthonormal residuals without Gaussian transformation

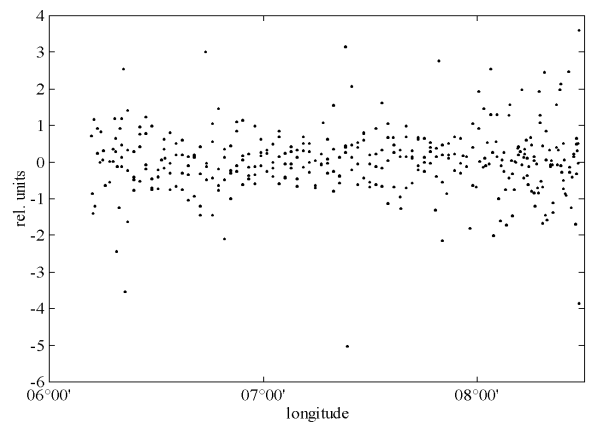


Fig. 9: Orthonormal residuals after Gaussian transformation.

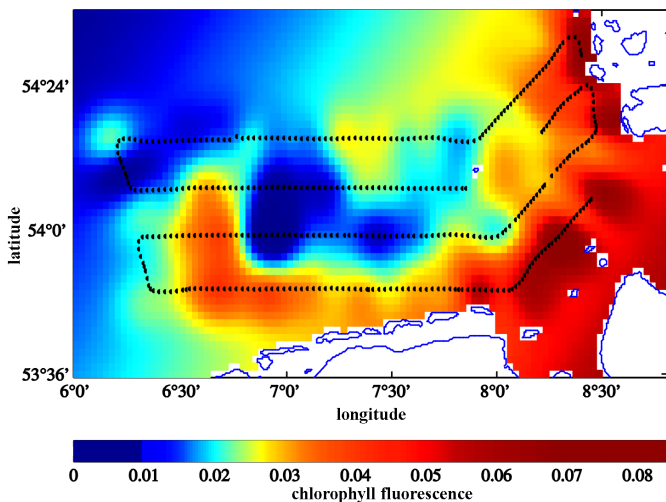


Fig. 10: Kriging predictor of the distribution of chlorophyll fluorescence in the German Bight, relative units. Excitation at 308 nm, emission at 685 nm. Survey on Sept 13th., 1995 (see Fig 2).

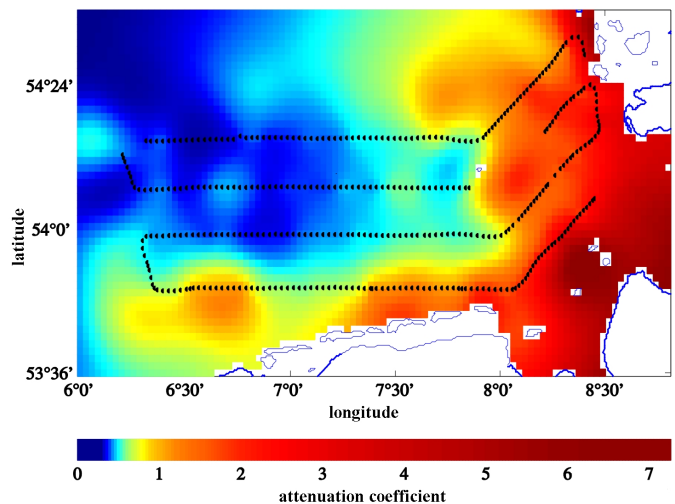


Fig. 11: Kriging predictor of the distribution of the attenuation coefficient (308 nm+344 nm)/2, derived by inversion of the water Raman scatter signal at 344 nm with excitation at 308 nm, in relative units.

The data set has been reduced to 400 values to simplify the following computations. The variogram parameters are estimated with the RML method, considering a quadratic trend in west/east-orientation. The experimental semivariogram is fitted by a Gaussian model with an additive nugget effect. The spatial distribution of the data positions does not allow to obtain a reliable estimation of an anisotropic semivariogram.

The kriging estimator and prediction variance of gelbstoff fluorescence is shown in Figs. 4 and 5. Besides the error introduced by the trend estimation, the prediction variance is a pure function of the spatial distance from the flight track. The increasing data variance near the coastline has no effect. The orthogonal residuals plotted versus the longitude in Fig. 6 emphasise this inadequate representation of the data by the model.

These results have to be compared to estimated distributions calculated with a previous application of a Gaussian transformation. The optimal value of the Box-Cox parameter ρ for the gelbstoff transformation is -0.88. The transformation simplifies the trend fitting, because the strong eastwards increase of the data is weakened and a linear trend model is adequate to the data. The variogram parameters again were estimated by maximising the RML.

The results of the kriging estimator and the difference between the quantiles $Q(0.84)$ and $Q(0.16)$ are shown in Figs. 7 and 8. The estimation uncertainty now clearly increases towards the east. To underline the improvement of the results a plot of the orthogonal residuals versus the longitude is presented in Fig. 9. The distribution of the residuals is almost uniform.

The distribution of chlorophyll fluorescence from algae and of the attenuation coefficient, measured in the same mission of the aircraft, is shown in Figs. 10 and 11. These data are derived simultaneously to gelbstoff by analysing the chlorophyll fluorescence peak and the intensity of water Raman scattering in the fluorescence spectrum (Fig. 1).

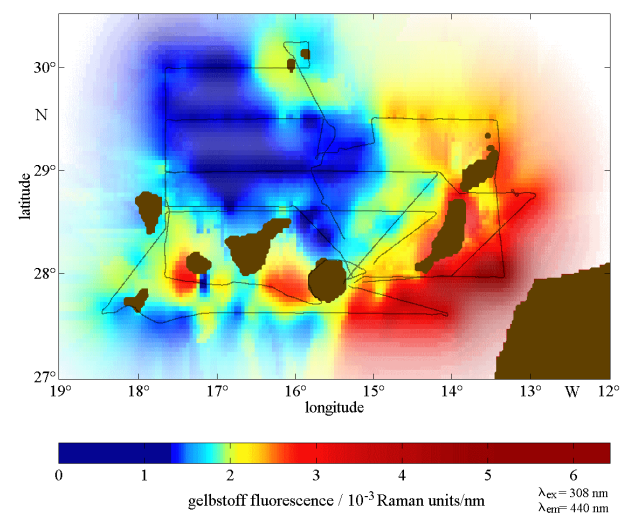


Fig. 12: Kriging predictor (colour) and uncertainty (brightness) of the gelbstoff distribution in the Canary Islands region, measured on June 3rd-6th, 1995. Dotted lines: flight tracks.

Results of a campaign in the region of the Canary Islands are another example of airborne laser fluorosensor measurements (Fig. 12). The distribution of gelbstoff fluorescence is low in the open sea, mainly due to photodegradation of fluorophores as a result of

intense sunlight. Data are high near the African coast and south of the islands. This effect is caused by upwelling of water from about 100 to 500 m depth, i.e. is from below the photic zone, from which result higher amounts of undegraded fluorophores in the near-surface water layer.

The airborne fluorescence data are calibrated with samples analysed in the ship laboratory as the ground truth, and given in Raman units, i.e. normalised to the integral of the water Raman scatter band.^{13,14} In this figure, a combined presentation of kriging predictor and uncertainty has been realised by associating the predictor with a specific colour and the accuracy of a predicted signal with the brightness of the same colour. This kind of visualisation seems to be most appropriate since it provides an information on the quantity of a parameter and its accuracy in the same image.

4. CONCLUSION

Geostatistical methods have proven to be a powerful set of tools for data analysis and interpolation, although there are some restrictions in their application if spatial statistical homogeneity of the data does not hold. In this paper we discuss the Box-Cox transformation to multivariate normality as a strategy to cope with this problem.

A practical application is presented where these transformations were used with success. Especially the distribution of the prediction variance seems to be much more realistic. This can be proven by the orthogonal residuals that show almost no spatial dependence, in contrast to the residuals calculated with the standard kriging routine.

5. ACKNOWLEDGEMENTS

We are grateful to the pilots and operators from the Naval Air Wing 5 in Nordholz, Germany, for their support in measuring maritime parameters in parallel to maritime pollution surveillance. Operation of the aircraft is financed by the Ministry of Transport and the Ministry of Defence. The laser fluorosensor (LFS) has been developed with support from the Ministry of Research and Technology.

6. REFERENCES

1. K. Grüner, R. Reuter and H. Smid, „A new sensor system for airborne measurements of maritime pollution and of hydrographic parameters“, *GeoJournal*, 24.1: 103-117, 1991.
2. R. Reuter, H. Wang, R. Willkomm, K. Loquay, T. Hengstermann, and A. Braun, „A laser fluorosensor for maritime surveillance: Measurement of oil spills“, *EARSel Advances in Remote Sensing* 3: 152-169, 1995.

3. T. Hengstermann, and R. Reuter: “Laser Remote sensing of pollution of the sea: a quantitative approach.” *EARSel. Advances in Remote Sensing* 1: 52-60, 1992.
4. R.M. Measures, „Laser Remote Sensing. Fundamentals and Applications“, John Wiley & Sons, New York 1984.
5. R. Reuter, D. Diebel, and T. Hengstermann, „Oceanographic laser remote sensing; measurements of hydrographic fronts in the German Bight and in the northern Adriatic Sea“, *International Journal of Remote Sensing* 14: 823-848, 1993.
6. A.G. Journel, and C.J. Huijbregts, „Mining Geostatistics“, Academic Press, New York 1978.
7. E. Isaacs, and M. R. Srivastava, „An Introduction to Applied Geostatistics“, Oxford University Press, New York 1989.
8. C.V. Deutsch, and A. G. Journel, „GSLIB: Geostatistical Software Library and User’s Guide“, Oxford University Press, New York 1992.
9. P.K. Kitanidis, and R.W. Lane, „Maximum likelihood parameter estimation of hydrologic spatial processes by the Gauss-Newton-method“, *Journal of Hydrology* 79: 53-71, 1985.
10. N.R. Draper, and H. Smith, „Applied Regression Analysis“, John Wiley and Sons, New York 1981.
11. P.K. Kitanidis, „Orthonormal residuals in geostatistics: Model criticism and parameter estimation“, *Mathematical Geology* 25: 741-758, 1991.
12. L.R. Poole, and W.E. Esaias, „Water Raman normalization of airborne laser fluorosensor measurements: a computer model study“, *Applied Optics* 21: 3756-3761, 1982.
13. S. Determann, R. Reuter, P. Wagner und R. Willkomm: Fluorescent matter in the eastern Atlantic Ocean. Part 1: method of measurement and near-surface distribution. *Deep-Sea Research I*, 41: 659-675, 1994.